The Role of Higher Lying Electronic States in Charge Photogeneration in Organic Solar Cells

Giulia Grancini, Maddalena Binda, Stefanie Neutzner, Luigino Criante, Vittorio Sala, Alberto Tagliaferri, and Guglielmo Lanzani**

The role of excess photon energy on charge generation efficiency in bulk heterojunction solar cells is still an open issue for the organic photovoltaic community. Here, the spectral dependence of the internal quantum efficiency (IQE) for a poly[2,6-(4,4-bis-(2-ethylhexyl)-4*H*-cyclopenta[2,1-b;3,4-b]dithiophene)-alt-4,7-(2,1,3-benzothiadiazole)]:6,6-phenyl-C_{61}-butyric acid methyl ester (PCPDTBT:PC60BM)-based solar cell is derived combining accurate optoelectronic characterization and comprehensive optical modeling. This joint approach is shown to be essential to get reliable values of the IQE. Photons with energy higher than the bandgap of the donor material can effectively contribute to enhance the IQE of the solar cell. This holds true independently of the device architecture, reflecting an intrinsic property of the active material. Moreover, the nanomorphology of the bulk heterojunction plays a crucial role in determining the IQE spectral dependence: the coarser and more crystalline, the lesser the gain in IQE upon high energy excitation.

1. Introduction

In organic photovoltaic blends, charge generation is a multi-step process: the absorbed photon generates a singlet excited state that can further dissociate, upon diffusion to the donor acceptor interface, into a pair of opposite charge carriers.[1–4] A fraction of these carriers is eventually collected at the electrodes generating a current. If the nascent neutral excited state lies high in energy, it can first thermalize, by internal conversion (IC) and internal vibrational distribution (IVR), to the lowest singlet state and then dissociate (the cold dissociation process) or it can dissociate before thermalization (hot exciton dissociation). In the first case, excess energy is lost and the system does not have memory of the photon energy, except for a possible local increase of temperature.[5] The second case is expected in disordered semiconductors, where the distance between the resulting charge carriers is a sub-linear function of the excess photon energy.[6] A requisite for hot dissociation to occur is that the dissociation rate should be faster than both, IC and IVR. When this happens, the split pair of charges may retain some or all the excess energy with respect to the lowest excited state, in the form of kinetic energy or potential energy.[2,7–9] Ultimately this energy may assist full charge separation.[7–9] Hot dissociation has indeed been observed in the ultrafast timescale for a blend of low-bandgap poly[2,6-(4,4-bis-(2-ethylhexyl)-4*H*-cyclopenta[2,1-b;3,4-b]-dithiophene)-alt-4,7-(2,1,3-benzothiadiazole)] (PCPDTBT) donor and fullerene acceptor.[10] If the charge pair formed by hot dissociation has a higher chance to escape recombination, perhaps proportional to the amount of excess energy involved, hot dissociation would lead to a higher quantum efficiency of charge generation for higher photon energy. The latter is however a highly debated question.[11–17]

The main spectral figure of a solar cell is the external quantum efficiency (EQE). EQE is defined as the ratio of the charge carriers collected by the device to the number of incident photons of a given energy. The EQE does not provide specific information on the losses in the device or the role of different layers. The internal quantum efficiency (IQE), i.e., the fraction of extracted electrons per absorbed photon, on the contrary, gives an insight into the charge generation process. As is, it would still be a property of the device, corrected for reflection, diffusion and eventually transmission of incident light. It is however common use to define IQE for the active layer only, i.e., IQE is the ratio between the number of extracted electrons and the number of the absorbed photons in the active layer. This strict definition implies that measuring the IQE is difficult, since the isolated absorption of the active material within a full device structure is not a directly experimentally accessible quantity.[17] Although the absolute value of the IQE depends on the specific device structure, encompassing the effects of internal fields, transport, recombination and collection of charge carriers, its spectral shape yields important information about the active material. Notably device-related effects, as mentioned above, should have a weak dependence on the initial photon energy. Therefore, characteristic features observed in the spectral shape can be confidently attributed to the properties of the active layer.

Dr. G. Grancini, Dr. M. Binda, S. Neutzner,
Dr. L. Criante, Prof. G. Lanzani
Center for Nano Science and Technology@Polimi
Istituto Italiano di Tecnologia
via Giovanni Pascoli 70/3, 20133 Milan, Italy
E-mail: giulia.grancini@epfl.ch; guglielmo.lanzani@iit.it
S. Neutzner, V. Sala, Prof. A. Tagliaferri, Prof. G. Lanzani
Dipartimento di Fisica
Politecnico di Milano
Piazza L. da Vinci, 32, 20133 Milan, Italy

DOI: 10.1002/adfm.201501873

For energy conversion, the crucial point is the final outcome of hot dissociation over quantum efficiency. Hot dissociation could occur but still be irrelevant if the nascent charge pair does not bear any memory of the initial excess energy (e.g., a fixed intercharge distance) or loses its energy before any further step towards separation.[9] For this reason, measuring the IQE seems the crucial step to assess the role of hot dissociation in photovoltaic bulk heterojunction (BHJ).

Here, we report on a detailed investigation of the IQE in photovoltaic cells based on PCPDTBT/6,6-phenyl-C_{61}-butyric acid methyl ester (PC60BM) (1:3) as an active layer blend. We find that the IQE has a week dependence within the lowest singlet vibronic manifold, down to about 550 nm, and start to rise at shorter wavelengths, when higher electronic levels (S2 and S4,[10] are progressively excited).

2. Results

Figure 1a,c shows the sketches of the vertical device structures that we investigated. In addition, as presented later, we also explore a planar structure with interdigitated electrodes. We compare two vertical architectures differing for the presence of the PEDOT:PSS layer, which is commonly used in devices to improve the cell performance. Our goal is to investigate how the interfacial charge generation process is affected by the active layer morphology. To optimize the charge generation efficiency, we use a blend with small domains size that has the highest interface extent at the expense of transport performance. To obtain this, we avoid the use of additives, reported in the literature as a tool to enhance phase segregation,[18] and we do not apply any thermal annealing to the deposited film. In order to correctly evaluate the optical absorption of the active layer within the stack, that is essential to derive the information on the IQE, we measure the thickness of all the individual layers by means of 5 kV cross-sectional scanning electron microscopy (SEM) image (≈5 nm lateral resolution) directly on the device. As shown in Figure 1b,d, the active layer, 150 nm thick, is in both cases uniform and smooth with a surface roughness comparable to our resolution.

Standard setups for EQE measurements are usually based on a white lamp coupled into a monochromator to generate monochromatic light stimulation of the device. As a result, the light spectrum impinging on the device is given by the convolution of the lamp emission spectrum with the monochromator transmission. Moreover, these setups generally make use of lenses that are affected by severe chromatic aberration. As a consequence, the excitation intensity is far from constant over the spectral range. This yields a spurious dependence of the photogenerated charge density on the excitation wavelength, contributing to often misevaluate the spectral shape of the IQE. On the other hand, the photocurrent transient behavior is typically not monitored by such systems, while the correct evaluation of the extracted carriers must be done at steady-state conditions. In order to circumvent these limitations, that are overlooked in most published work,[11,16] in our measurements the devices were stimulated with pulsed LED monochromatic light over a 405–840 nm range. The corresponding device photocurrent in short-circuit condition (J_{SC}, A mm^{-2}) was read by a transimpedance amplifier and recorded with an oscilloscope. The impinging light intensity (I, W mm^{-2}) at each wavelength was calibrated by means of a silicon photodiode (Siemens BPX-65) having the same photoactive area (dimension and shape) as the device under test (1 mm^2). This represents a key point, often neglected, to ensure high precision of the calibration regardless the spatial uniformity features of the incident light beam. A simulated light absorption profile in the active material was

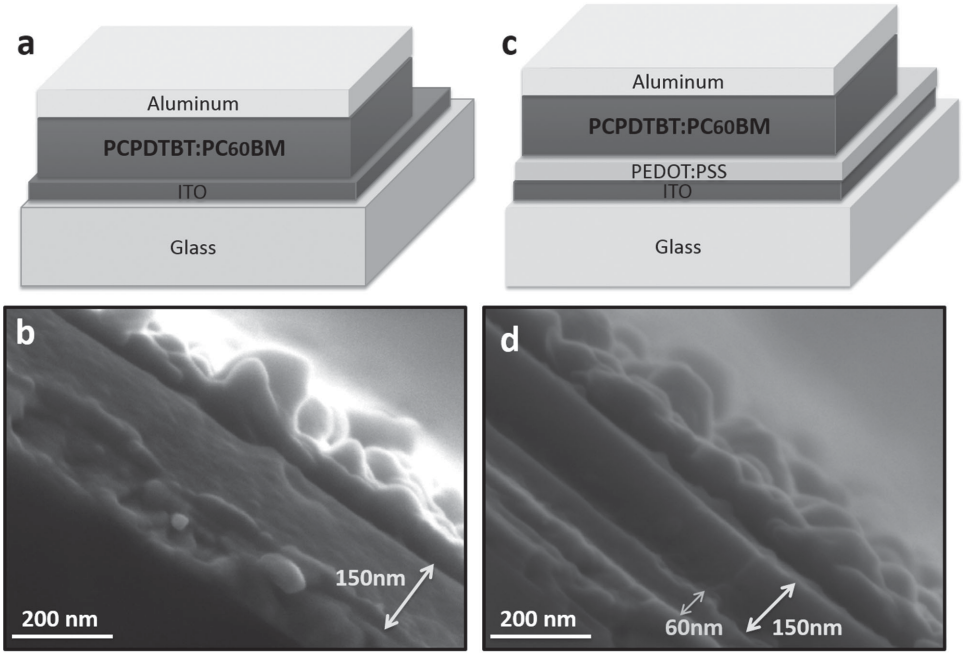

Figure 1. a,c) Sketch of the device architecture; b,d) high-resolution SEM images of the device cross section, the arrows indicate the active layer (150 nm) and the PEDOT:PSS layer (60 nm).

used to set the LEDs intensity in order to ensure comparable photogenerated charge density at each wavelength across the measurement range. The transient behavior of the photocurrent signal is monitored and the steady-state value is taken for calculation of the EQE. The EQE of the devices was then given by: EQE (%) = 100 · (1240 · J_{SC}) / (λ [nm] · I), with obvious meanings of the various parameters, as described previously. All the electrical measurements were carried out in high vacuum (≈10^{-6} mbar) to remove any possible artifact due to oxygen and moisture contamination.

Figure 2 shows the extracted EQE for the devices under investigation. In fair agreement with data reported in literature,[11] values around 20% at the absorption peak have been obtained, slightly higher for the case with PEDOT:PSS layer.

To extract the IQE, the EQE must be divided by the fraction of light absorbed by the active layer only (Abs_{AL}) as: IQE(λ) = EQE(λ)/Abs_{AL}.

Different methods can be used to obtain Abs_{AL}, including simulation only or a combination of modeling and experiments leading a more accurate value, from which different IQE(λ) spectra can be derived.[17] In particular, three different cases can be evaluated, as shown in **Figure 3**: i) one can rely on the simulated absorption of the active layer within the stack (Figure 3a). The transfer matrix method (TTM) is a computing technique usually applied to simulate complex multilayer structures (with layer thicknesses comparable to the visible wavelength).[17] In such simulation, a multilayer is a stack of homogeneous thin films with different indices of refraction that can be modeled assuming the invariance of dielectric properties with respect to continuous translation in two orthogonal directions and not in the third one. The basic formalism provides the amplitude of the electromagnetic field of monochromatic waves reflected by and transmitted through the mentioned multilayered structure. The solution is achieved through propagation of the fields in the homogeneous layers constituting the structure, and applying the proper boundary conditions at their interface. Each layer is described in terms of its (coherent) wave propagation coefficient and interface matrix, considering the complex refractive index of the materials, the layer thicknesses as well as the incidence angle and polarization of the incident light. With the exception of approximations in the chosen model, i.e., simplified dimensionality and initial conditions, this analytical method is exact. Therefore, it takes into account all the electromagnetic field effect within the thin layer structure as the destructively or constructively interference effects, if occurred, of the electromagnetic wave. Reflection and transmission of the thick glass substrate is treated incoherently (transmission and reflection of a slab approximated as an infinite medium) and included in the algorithm. The simulated absorption of the active layer ($Abs_{AL\text{-}Sim}$) is presented for the two architectures in Figure 3a ($Abs_{AL\text{-}sim}$, parametric on the active layer thicknesses are shown in Figure S1, Supporting Information). Note that the PEDOT:PSS layer introduces a non-negligible contribution to the interference effects, thus explaining the difference in magnitude of the active layer absorption. The derived IQE is shown in Figure 3d; ii) in the previous approach, the exact knowledge of the complex dielectric tensor of the stack is crucial. In order to overcome the experimental uncertainty of these parameters, which are notoriously difficult to measure, we follow the

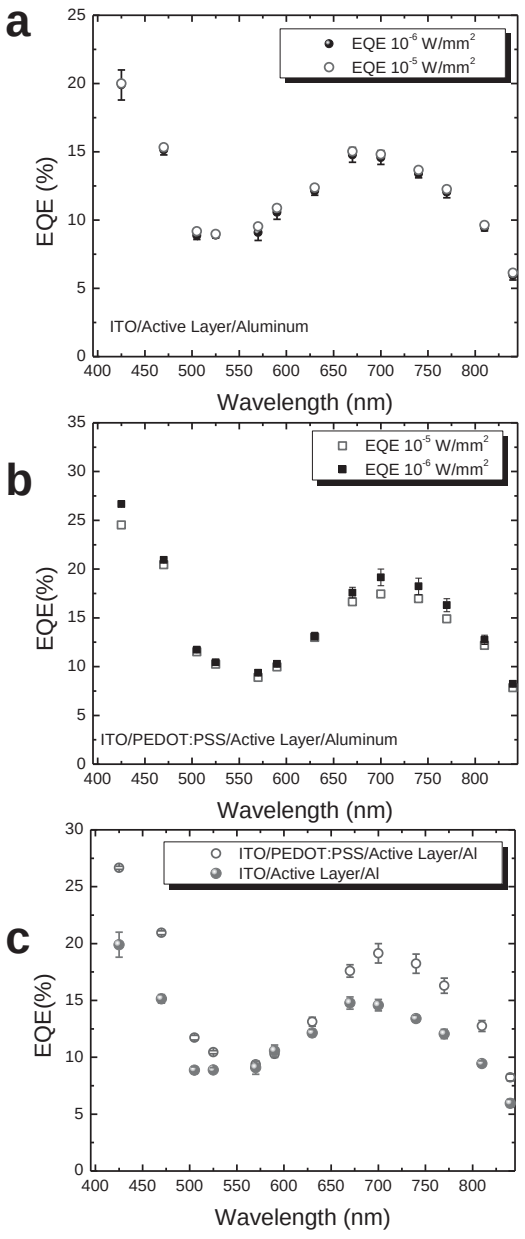

Figure 2. External quantum efficiency (EQE) measurements on a) ITO/PCPDTBT:PC60BM/Al and b) ITO/PEDOT:PSS/PCPDTBT:PC60BM/Al vertical device. In order to rule out any possible charge-density-dependent effect, we kept equal the number of absorbed photons per each wavelength and we repeated the measurement at two different ranges of light intensity; c) comparison of the EQE for the different architectures with and without PEDOT:PSS layer. Error bars: statistic on a series of 10 devices.

method proposed by Burkhard et al.[17] that minimizes this error by using the TTM model to calculate the parasitic absorption (PA). PA is defined as the absorption by all the layers that do not contribute to the photocurrent. A thickness dependence of PA is calculated and shown in **Figure 4**a,b. By subtracting this from the experimentally measured total device reflectance (R), shown in Figure 4c,d, one obtains Abs_{AL} = 1 − PA − R. Note that because R is highly accurate, errors in the resulting

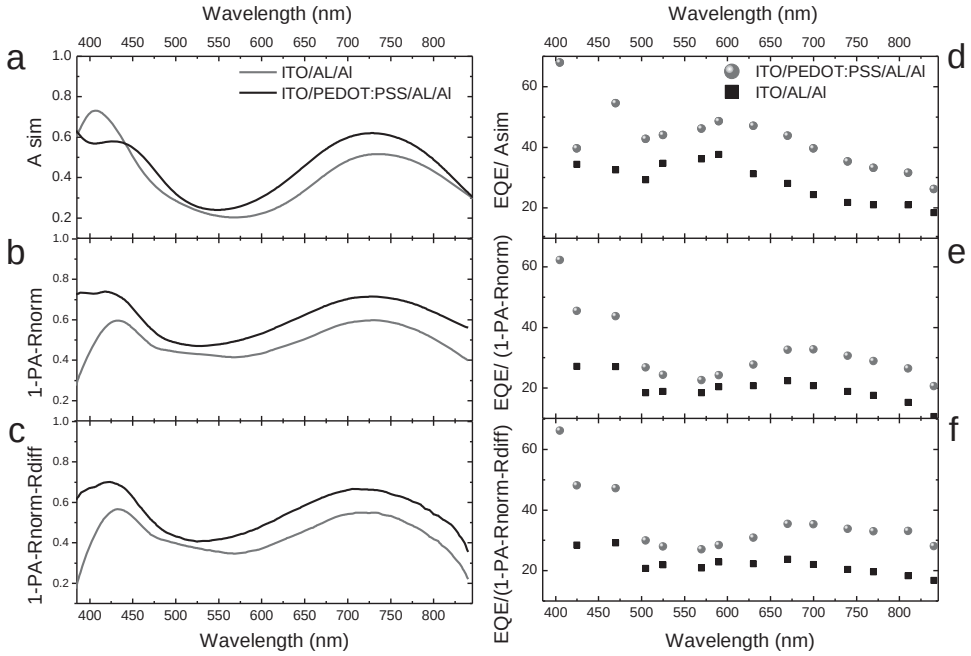

Figure 3. Active layer absorption for the two device architectures with and w/o PEDOT:PSS layer using a) simulated absorption; b) 1-simulated parasitic absorption (PA)—measured reflectance at normal direction (R_{norm}); c) 1 − PA − R_{norm}-scattered component (R diff); d–f) IQE derived by dividing the measured EQE by the absorption as in (a–c).

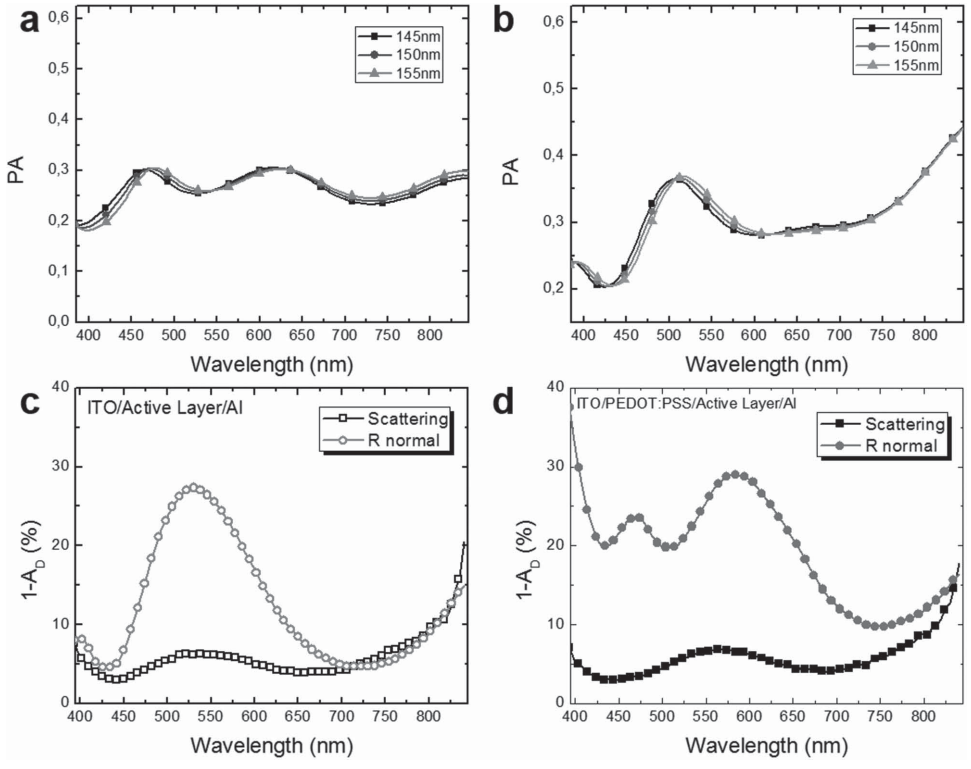

Figure 4. a,b) Calculated parasitic absorption (PA) for three different thicknesses of the active layer as in the legend for the device w/o and with PEDOT:PSS layer, respectively. PA = Absorption of light in all the stack of the device, except the active layer. c,d) Normal and diffuse reflectance spectra for the device w/o and with the PEDOT:PSS layer, respectively.

Abs_{AL} are only as small as the small errors in the PA, loosening the requirements for the accuracy of the optical constants of the blend.[17] In this way, we obtain the IQE shape reported in Figure 3e; iii) in the literature R is usually measured only at near-normal condition (R_{norm}) while the diffuse scattering and the spatially dependent optical constants of the blend layer are not taken into account.[11,16] To further improve the analysis, we use a home-made system that allows us to simultaneously get the near-normal incidence reflectance spectra and the effective losses of the sample (as in Figure 4c,d). This allows accounting for second-order phenomena such as optical scattering from rough film surfaces and interfaces, that are usually neglected,[11,16] and the amount of incident light power "guided" in the substrate toward its edges that never reach the absorbent layer. The latter component is closely related to the substrate thickness. This last method leads to IQE as reported in Figure 3f.

The IQE plots reported in Figure 3 all display a rising trend with reducing wavelength (from around 15% in the red region to approximately 30% in the blue region). Such discrete wavelengths spectra are highly accurate, yet the rising component is identified only by two experimental points. We thus turn to a continuous light source, using the LED-based measurement as a test to validate the calibration upon excitation density dependence, which is harder when using the lamp. In **Figure 5**, our best IQE obtained by using the LED set-up is compared with that measured by using a monochromated lamp (solid line). The two sets of data are consistent within the confidence range.

To sum up, the measured IQE suggests that higher lying electronic states are keener to generate charge carriers and to contribute to the photocurrent, in agreement with other results and notably with a recent investigation based on electric field saturation.[19,20]

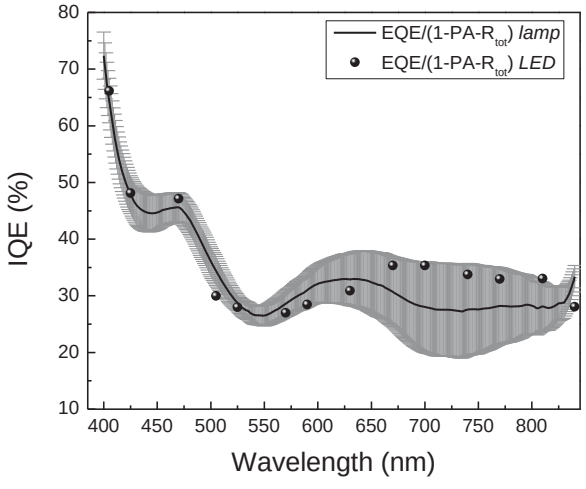

Figure 5. IQE derived by dividing by $(1 - PA - R_{norm} - R_{diff})$ the measured EQE obtained by using the LED set-up (with equalized number of absorbed photons at each wavelength) and obtained by using a standard set-up based on monochromated lamp (solid line). The gray area defines the interval of confidence evaluated considering the error bar for each measurement. In particular, the relative variation (grey line) is defined by: $\Delta IQE = dIQE/dEQE \times \Delta EQE + dIQE/dPA \times \Delta PA + dIQE/dR \times \Delta R$, thus $\Delta = ([1/(1 - PA - R)) \times \Delta EQE]^2 + [EQE/(1 - PA - R)^2 \times \Delta PA]^2 + [EQE/(1 - PA - R)^2 \times \Delta R]^2)^{0.5}$.

3. Discussion

The observation of hot dissociation in the ultrafast time scale, as reported earlier, is a reasonable explanation for the increasing IQE at higher excitation energy. Hot dissociation would somehow exploit excess energy for enhanced charge separation. However we should first consider other possible interpretations for the high energy increase of the IQE. Perhaps the most relevant is the role of PC60BM. Upon raising photon energy, absorption within PC60BM molecules augments. This might be followed by hole transfer to the polymer and contribute to the photocurrent. In order for this to explain the observed trend, one should assume that there is a higher efficiency for hole transfer from PC60BM to the polymer than for the electron transfer from the polymer to PC60BM. The later has never been reported and seems unlikely because hole transfer occurs in the 100 ps time scale in P3HT:PC60BM blend,[21] while electron transfer is much faster. In addition, on the ultrafast time scale, changing the PC60BM concentration does not affect the dynamics,[10] suggesting that PC60BM is not involved in the hot process. Based on this observation not only the absorption in PC60BM should be ruled out as an explanation for a higher IQE, but it should be considered that this may have an opposite effect: a less effective charge separation following absorption into PC60BM would lead to a decrease of the IQE, masking the hot dissociation effect.

The model of charge generation in disordered semiconductors, where localized states are distributed into an incoherent energy band, could offer a simple explanation for the energy-dependent IQE.[6] Larger excess energy leads to a larger separation distance within the initial charge pair, which has a higher escape probability, according to the Onsager or Braun–Onsager model.[7,8] For a donor/acceptor blend, such a model is however questionable, as the initial charge separation distance is assumed to be that of the D/A separation. This implicitly assumes a cold dissociation model, as in the Popovic–Noolandi–Hong theory.[22,23] Recently, however, a growing body of evidence suggests that the nascent pair is delocalized beyond the nearest neighbor distance[24–26] and points to the role of excess energy even at the donor/acceptor interface. Particularly relevant for our discussion is the very recent report[20] on the decrease in the extraction field saturation (defined as the electric field for 100% charge carrier quantum yield) upon increasing the excitation energy. This is an indication that pairs formed after higher energy excitations are less bounded. Several phenomena may explain the reduced binding energy following a "hot" process. Higher lying states in the donor polymer are more delocalized.[20] This implies a lower binding energy and a higher yield of dissociation into less-bounded pairs. Higher lying states have access to higher density of states that boosts the dissociation rate and couples to more delocalized charge pairs. IC from a higher lying state dissipates more energy and may lead to a higher local temperature that in turn can favor charge carrier escape. At this regard, however, it should be noted that excitation within the first vibronic band does not seem to lead to an energy-dependent IQE, suggesting that it is not just a matter of excess energy and eventually local temperature, but rather a more subtle effect, linked to the nature of the electronic states. This is indeed changing while going higher

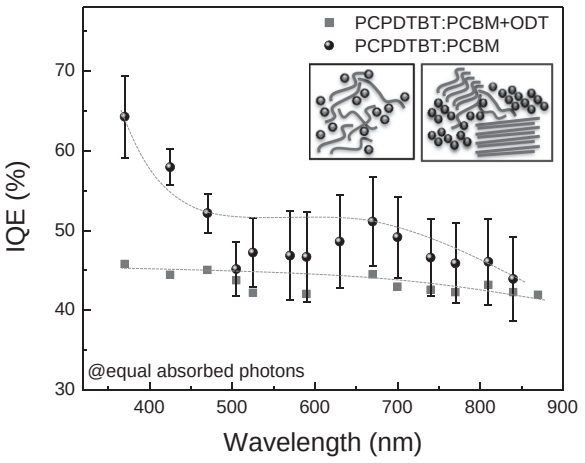

Figure 6. IQE derived by dividing the measured EQE obtained by using the LED on a planar device based on a PCPDTBT:PC60BM blend (error bar is related to the uncertainty on the thickness of the active materials of ±10 nm) or a PCPDTBT:PC60BM+ODT blend at equal absorbed photons condition for each wavelength. Dashed lines only represent an eye-guideline.

in energy, thereby increasing the ionic character and the wavefunction delocalization of the state.

It seems that in many studies on the IQE the energy dependence is overlooked.[11,16,27] In the correspondence appeared in ref. [27], the proposed plot for the IQE is squeezed by the scale, and a dependence on energy difficult to appreciate. A proper rescaling of the same data however shows exactly the same behavior that we report here. In other works, the IQE is reported in log scale over many orders of magnitude, obscuring the rise at high energy. Furthermore when large extraction fields are used to collect the photogenerated charges the eventual distribution in binding energy is washed out. Finally it should be taken into account that morphology is affecting generation, transport, and recombination, thus becoming responsible for a certain spread in experimental results. Transport is very important in planar devices that are in principle a simple system to be investigated. Also in a planar device however, after careful calibration of all possible artifacts, we measure consistently a rise of the IQE (**Figure 6**). On the contrary when using an additive that changes the morphology towards larger domains with reduced extension of donor/acceptor interfaces, we obtain a virtually flat IQE (shown in Figure 6). This very well demonstrates the role of morphology.

4. Conclusion

The IQE in polymer BHJs with small domain morphology increases upon excitation of higher lying singlet electronic states. This might be associated with hot dissociation, occurring before energy relaxation and leading to a less-bounded charge pair. The outcome is well consistent with standard pictures for charge generation in disordered semiconductors and molecular solids, and finds large agreement with other recently published experiments and theory. This suggests that hot dissociation of higher lying states may play a role and possibly be considered when designing new organic photovoltaic cells.

5. Experimental Section

Device Fabrication: Vertical devices were fabricated on glass substrates with prepatterned ITO electrodes (Xin Yan Technology LTD., 15 Ω/□). Before the PEDOT:PSS deposition and after accurate cleaning in bidistilled water, acetone, and isopropanol, substrates underwent O_2 plasma treatment. PEDOT:PSS (Clevios 4083) was deposited by spin coating at 2000 rpm from 0.2 μm PVDF filtered solution. Thermal annealing at 110 °C for 15 min in nitrogen atmosphere was performed. The 1:3.7 by weight PCPDTBT:PC60BM solution, with a concentration of 10 mg mL^{-1}, was spun cast at 1000 rpm. The aluminum cathode was thermally evaporated through a suitable shadow mask giving a pixel active area of 1 mm^2.

Planar devices were realized by spin casting the blend with the same recipe as for vertical devices onto fused silica substrates provided with prepatterned interdigitated gold electrodes with a channel length of 6 μm. In the case of devices provided with an additive to increase phase segregation, 1-octadecanethiol was added to the blend solution (4% by volume).

Scanning Electron Microscopy Measurements: A Tescan MIRA3 SEM was used for scanning electron microscopy imaging. The pictures was acquired by the in-column secondary electron detector with the following parameter: acceleration voltage 5 kV, beam current of about 10 pA, working distance 0.5 mm, and acquisition times ranging from 30 s to a couple of minutes.

Diffuse Reflectance Measurements: To measure the reflectance, both normal and effective diffusive components simultaneously, a home-made system was developed. It was based on fiber optic reflection probe coupled into an integrating sphere. It had one illuminating fiber in the center surrounded by six fibers able to collect the device normal reflectance. The seven individual fibers were multimodal (0.22 NA) and transmission in the 350–2000 nm spectral ranges. The special probe, which had been placed within the integrating sphere very close and at normal position with respect to the device surface, allowed maintaining an incident plane wave condition until a few mm from the tip (working distance). The shining light uniformly illuminated the sample area. On the same time, the integrating sphere, coupled with a standard spectrofluorimeter (*NanoLog Horiba Jobin Yvon*) was used to collect the diffuse component.

Supporting Information

Supporting Information is available from the Wiley Online Library or from the author.

Acknowledgements

G.G. and M.B. contributed equally to this work. The authors thank Dr. Stefano Perissinotto for the help with the absorption/reflectance measurements and Dr. Maurizio Zani for the help with the SEM measurements. The authors also acknowledge Carlo Brambilla and Mauro Scarparo for the help in the fabrication of the home-made setup for reflection measurements. The research leading to these results has received funding from the European Union's Horizon 2020 research and innovation programme under the Marie-Sklodowska-Curie grant agreement No 643238.

Received: May 6, 2015
Revised: August 28, 2015
Published online: October 15, 2015

[1] H. Hoppe, N. S. Sariciftci, *J. Mater. Res.* **2004**, *19*, 1924.
[2] G. Lanzani, *The Photophysics Behind Photovoltaics and Photonics*, Wiley-VCH, Weinheim, Germany **2012**.
[3] T. M. Clarke, J. R. Durrant, *Chem. Rev.* **2010**, *110*, 6736.
[4] G. Grancini, D. Polli, D. Fazzi, J. Cabanillas-Gonzalez, G. Cerullo, G. Lanzani, *J. Phys. Chem. Lett.* **2011**, *2*, 1099.
[5] V. I. Arkhipov, E. V. Emelianova, H. Bässler, *Phys. Rev. Lett.* **1999**, *82*, 1321.
[6] D. M. Pai, R. C. Enk, *Phys. Rev. B* **1975**, *11*, 5163.
[7] L. Onsager, *J. Chem. Phys.* **1934**, *2*, 599.
[8] C. L. Braun, *J. Chem. Phys.* **1984**, *80*, 4157.
[9] D. Fazzi, G. Grancini, M. Maiuri, D. Brida, G. Cerullo, G. Lanzani, *Phys. Chem. Chem. Phys.* **2012**, *14*, 6367.
[10] G. Grancini, M. Maiuri, D. Fazzi, A. Petrozza, H.-J. Egelhaaf, D. Brida, G. Cerullo, G. Lanzani, *Nat. Mater.* **2013**, *12*, 29.
[11] A. Armin, M. Velusamy, P. Wolfer, Y. Zhang, P. L. Burn, P. Meredith, A. Pivrikas, *ACS Photonics* **2014**, *1*, 173.
[12] G. Grancini, M. Binda, L. Criante, S. Perissinotto, M. Maiuri, D. Fazzi, A. Petrozza, H.-J. Egelhaaf, D. Brida, G. Cerullo, G. Lanzani, *Nat. Mater.* **2013**, *12*, 594.
[13] S. D. Dimitrov, J. R. Durrant, *Chem. Mater.* **2014**, *26*, 616.
[14] A. A. Bakulin, A. Rao, V. G. Pavelyev, P. H. M. van Loosdrecht, M. S. Pshenichnikov, D. Niedzialek, J. Cornil, D. Beljonne, R. H. Friend, *Science* **2012**, *335*, 1340.
[15] K. Vandewal, S. Albrecht, E. T. Hoke, K. R. Graham, J. Widmer, J. D. Douglas, M. Schubert, W. R. Mateker, J. T. Bloking, G. F. Burkhard, A. Sellinger, J. M. J. Fréchet, A. Amassian, M. K. Riede, M. D. McGehee, D. Neher, A. Salleo, *Nat. Mater.* **2014**, *13*, 63.
[16] A. Armin, I. Kassal, P. E. Shaw, M. Hambsch, M. Stolterfoht, D. M. Lyons, J. Li, Z. Shi, P. L. Burn, P. Meredith, *J. Am. Chem. Soc.* **2014**, *136*, 11465.
[17] G. F. Burkhard, E. T. Hoke, M. D. McGehee, *Adv. Mater.* **2010**, *22*, 3293.
[18] S. H. Park, A. Roy, S. Beaupré, S. Cho, N. Coates, J. S. Moon, D. Moses, M. Leclerc, K. Lee, A. J. Heeger, *Nat. Photonics* **2009**, *3*, 297.
[19] L. A. A. Pettersson, L. S. Roman, O. Inganäs, *J. Appl. Phys.* **1999**, *86*, 487.
[20] T. Hahn, J. Geiger, X. Blase, I. Duchemin, D. Niedzialek, S. Tscheuschner, D. Beljonne, H. Bässler, A. Köhler, *Adv. Funct. Mater.* **2015**, *25*, 1287.
[21] A. R. Srimath Kandada, G. Grancini, A. Petrozza, S. Perissinotto, D. Fazzi, S. S. Kumar Raavi, G. Lanzani, *Sci. Rep.* **2013**, *3*, 1.
[22] Z. Noolandi, K. M. Hong, *J. Chem. Phys.* **1979**, *70*, 3230.
[23] N. E. Geacintov, M. J. Pope, *Chem. Phys.* **1965**, *47*, 1194.
[24] A. E. Jailaubekov, A. P. Willard, J. R. Tritsch, W.-L. Chan, N. Sai, R. Gearba, L. G. Kaake, K. J. Williams, K. Leung, P. J. Rossky, X.-Y. Zhu, *Nat. Mater.* **2013**, *12*, 66.
[25] S. Gélinas, A. Rao, A. Kumar, S. L. Smith, A. W. Chin, J. Clark, T. S. van der Poll, G. C. Bazan, R. H. Friend, *Science* **2013**, *343*, 512.
[26] F. Provencher, N. Bérubé, A. W. Parker, G. M. Greetham, M. Towrie, C. Hellmann, M. Côté, N. Stingelin, C. Silva, S. C. Hayes, *Nat. Commun.* **2014**, *5*, 1.
[27] A. Armin, Y. Zhang, P. L. Burn, P. Meredith, A. Pivrikas, *Nat. Mater.* **2013**, *12*, 593.